Zhang and Ohta *NPG Asia Materials* (2023) 15:67
https://doi.org/10.1038/s41427-023-00520-w

NPG Asia Materials

REVIEW ARTICLE Open Access

Recent progress in thermoelectric layered cobalt oxide thin films

Yuqiao Zhang[1] and Hiromichi Ohta[2]

Abstract

Oxide-based thermoelectric materials that show a high figure of merit are promising because of their good chemical and thermal stabilities and their relative harmlessness compared with chalcogenide-based state-of-the-art thermoelectric materials. Although several high-*ZT* thermoelectric oxides (*ZT* > 1) have been reported thus far, their reliability levels are low due to the lack of careful observations of their stabilities at elevated temperatures. Herein, we review the epitaxial film growth and thermoelectric properties of representative p-type layered cobalt oxides: $Na_{3/4}CoO_2$, $Ca_{1/3}CoO_2$, $Sr_{1/3}CoO_2$, $Ba_{1/3}CoO_2$, and $Ca_3Co_4O_9$. Among these specimens, $Ba_{1/3}CoO_2$ and $Ca_3Co_4O_9$ are stable in air at elevated temperatures (~600 °C). The *ZT* of $Ba_{1/3}CoO_2$ reaches ~ 0.55 at 600 °C in air, which is reliable and the highest among thermoelectric oxides. Moreover, this value is comparable to those of p-type PbTe and p-type SiGe.

Thermoelectrics

Today, most energy resources are discharged as waste heat into the environment without being applied. Such exhaust heat reaches approximately 2/3 of the primary energy. Hence, thermoelectric energy conversion technology has attracted great attention for converting waste heat into electricity[1,2]. The principle of thermoelectric energy conversion was first discovered by T.J. Seebeck in 1821[3]. He found that a voltage is generated between two ends of a metal bar by introducing a temperature difference. Thus, when electric loads are connected at both ends of a metal bar, an electric current can be obtained. This phenomenon is called the Seebeck effect. Conversely, in 1834, J.C.A. Peltier discovered that heating or cooling of the junctions can occur during electric current application to a heterogeneous metal circuit. This phenomenon is called the Peltier effect, and it has been commercially applied in electronic refrigerators, among other applications.

Correspondence: Yuqiao Zhang(yuqiaozhang@ujs.edu.cn) or
Hiromichi Ohta(hiromichi.ohta@es.hokudai.ac.jp)
[1]Institute of Quantum and Sustainable Technology (IQST), School of Chemistry and Chemical Engineering, Jiangsu University, Zhenjiang 212013 Jiangsu, China
[2]Research Institute for Electronic Science, Hokkaido University, N20W10, Kita, Sapporo 001-0020, Japan

Generally, the performance of thermoelectric materials is evaluated in terms of a dimensionless figure of merit, $ZT = S^2 \cdot \sigma \cdot T \cdot \kappa^{-1}$, where Z is a figure of merit, T is the absolute temperature, S is the thermopower (≡ Seebeck coefficient), σ is the electrical conductivity, and κ is the thermal conductivity. The energy conversion efficiency from transforming the temperature difference into electricity increases as ZT increases. Thus, to realize efficient thermoelectric energy conversion, three physical properties are needed for thermoelectric materials: (1) low κ, which is needed to introduce a large temperature difference into both ends of the material; (2) high σ, which is needed to reduce the internal resistance of the material; and (3) high S, which is needed to obtain a high voltage.

The ZT values of practical thermoelectric materials, such as Bi_2Te_3 and PbTe, are ~1, which is the lowest value needed for practical applications[4,5]. Recently, several high-ZT materials ($ZT > 1$) have been developed sequentially based on heavy metal alloys, including SnSe, PbSe, GeTe, and oxychalcogenides (BiCuSeO)[5–17]. Since thermoelectric devices can directly convert a temperature difference into electricity, some automobile companies have developed thermoelectric-assisted hybrid automobiles[18–21] while considering the outside temperature of the exhaust pipe to be ~700 °C. However, these thermoelectric materials are not appealing, particularly when operating at such high temperatures, because decomposition, vaporization, and melting of the constituents can easily occur. Furthermore, the use of these heavy metals should be limited to specific environments, such as space, because they are mostly toxic, low in abundance as natural resources, and not environmentally benign.

To overcome these issues, metal oxides have attracted much attention as thermoelectric power generation materials at high temperatures based on their potential advantages over heavy metal alloys in terms of chemical and thermal robustness[22–24]. From the 1950s to the 1970s, there was a boom in the search for oxide thermoelectric materials. At this time, researchers in the United States used thermoelectric effects to investigate the intrinsic properties of grown oxide single crystals. Since the 1990s, the search for oxide thermoelectric materials, which originated in Japan, has spread all over the world, including in Europe, the United States, Asia, and India. To date, it has been reported that some oxides could exhibit parameters of $ZT > 1$, exceeding that of PbTe.

History of thermoelectric oxides

There is a long history of thermoelectric oxides. From the 1950s to the 1970s (1st boom), the thermoelectric properties of many simple conducting oxides, including CdO (1949, Hogarth et al.[25]), NiO (1957, Parravano[26]), ZnO (1959, Hutson[27]), In_2O_3 (1962, Arvin[28]), $SrTiO_3$ (1964, Frederikse et al.[29]), rutile-TiO_2 (1965, Thurber et al.[30]), SnO_2 (1965, Marley and Dockerty[31]), Cu_2O (1969, Young and Schwartz[32]), and Fe_3O_4 (1970, Griffiths et al.[33]), were studied to obtain the fundamental physical properties of conducting oxides, such as carrier effective mass. After the discovery of cuprous oxide-based high-T_c superconducting oxides in 1986[34], the thermoelectric properties of superconducting oxides, including La_2CuO_4 (1987, Cooper et al.[35]), La-Ba-Cu-O (1987, Chen et al.[36]), $YBa_2Cu_3O_{7-\delta}$ (1988, Lee et al.[37]), and Tl-Ca-Ba-Cu-O (1988, Mitra et al.[38]), were reported sequentially to clarify the superconducting transition (2nd boom).

After the research boom in the field of high-T_c superconductors, two Japanese researchers, Ohtaki and Terasaki, reported that oxides had good thermoelectric performance, including $CaMnO_3$ (1995, Ohtaki et al.[39]), Al-doped ZnO (1996, Ohtaki et al.[40]), and Na_xCoO_2 (1997, Terasaki et al.[41]). These reports triggered the 3rd boom of thermoelectric oxide research in the 2000s. As a result of energetic exploratory research on good thermoelectric oxides, $Ca_3Co_4O_9$ (2000, Masset et al.[42] and Funahashi et al.[43]) and electron-doped $SrTiO_3$ (2001, Okuda et al., La-doped[44], 2005, Ohta et al. Nb-doped[45,46]) were discovered. In 2012, Fergus reviewed the thermoelectric properties of promising oxides (mostly bulk ceramics), including $Ca_3Co_4O_9$, Na_xCoO_2, $SrTiO_3$, $CaMnO_3$, and ZnO[47] (also see the references therein). Recently, several scholars that have reported rather high ZT values for oxide ceramics. Acharya et al.[48] reported that $SrTi_{0.85}Nb_{0.15}O_3$ ceramics sintered with graphite flakes exhibit $ZT = 1.4$ at 1050 K, and Biswas et al.[49] reported that Al-doped ZnO ceramics sintered with reduced graphene oxide exhibit $ZT = 0.5$ at 1100 K. Although these reported ZTs are very attractive as practical thermoelectric materials, there is still no practical application for them, probably due to the low reliability of the ZT values.

To clarify the intrinsic thermoelectric properties of oxides, we focused on high-quality epitaxial films with stepped and terraced surfaces. As a result, we fabricated high-quality epitaxial films of several thermoelectric oxides, including $Na_{3/4}CoO_2$[50,51], $Sr_{1/3}CoO_2$[52], $Ca_{1/3}CoO_2$[53], $Ba_{1/3}CoO_2$[54], $Ca_3Co_4O_9$[53,55], $SrTiO_3$:Nb[46], TiO_2:Nb[56] and SrO($SrTiO_3$):Nb[57]. Among these oxides, we found that $Ba_{1/3}CoO_2$ epitaxial films exhibited a ZT value of ~0.55 at 600 °C in air, which is the highest and most reliable value among the reported thermoelectric oxides[54]. In this context, we reviewed the epitaxial film growth and thermoelectric properties of four representative p-type layered cobalt oxide films based on our efforts: $Na_{3/4}CoO_2$[50,51], $Sr_{1/3}CoO_2$[52], $Ca_{1/3}CoO_2$[53], and $Ba_{1/3}CoO_2$[54].

Epitaxial film growth of A_xCoO_2 (A_x = $Na_{3/4}$, $Ca_{1/3}$, $Sr_{1/3}$, and $Ba_{1/3}$)

$Na_{3/4}CoO_2$[50,51]

Figure 1 shows the schematic crystal structure of A_xCoO_2 (A_x = $Na_{3/4}$, $Ca_{1/3}$, $Sr_{1/3}$, and $Ba_{1/3}$). In the case of A_xCoO_2, the rigid CoO_2 layer and mobile A_x layer are alternately stacked along the c-axis. In 1997, Terasaki et al. discovered that a $NaCo_2O_4$ (≡Na_xCoO_2, $x \sim 3/4$) single crystal with a two-dimensional layered structure exhibits a very large power factor $S^2 \cdot \sigma$ of 5 mW m^{-1} K^{-2} in the in-plane direction at room temperature[41]. After this discovery, the electronic structure[58–60], crystal structure[61,62], and Na-composition dependence of the thermoelectric properties[62] of Na_xCoO_2 were energetically studied to understand the origin of the unusually large S. In 2001, Fujita and coworkers fabricated Na_xCoO_2 single crystals and reported that they exhibited ZT values of ~1.2 at 800 K[63]. This material has attracted much attention because it can be converted into a superconductor (T_c ~ 4.7 K) by introducing H_2O molecules into a layer between the two adjacent CoO_2^- layers[64].

To clarify the intrinsic thermoelectric properties of $Na_{3/4}CoO_2$, we fabricated thin epitaxial films of $Na_{3/4}CoO_2$. First, we tried to fabricate $Na_{3/4}CoO_2$ epitaxial films by the conventional pulsed laser deposition (PLD) technique, but we failed. Several reports have been written on the thin film growth of $Na_{3/4}CoO_2$ by PLD. However, the film quality in terms of crystallographic orientation, surface morphology, and lateral grain size is insufficient. In the case of $Na_{3/4}CoO_2$ film growth by PLD, it is very difficult to control the Na concentrations in the films at high temperatures in a vacuum environment due to the high vapor pressure of the Na species.

To overcome this difficulty, we modified the reactive solid-phase epitaxy (R-SPE)[50] method that was developed to fabricate single-crystal films of $InGaO_3(ZnO)_m$ (m = integer). Figure 2 schematically illustrates the R-SPE procedure. Step 1: A highly (111)-oriented CoO epitaxial film was deposited on a (0001)-α-Al_2O_3 substrate at 700 °C by the PLD technique using a Co_3O_4 sintered disk as a target. Step 2: The surface of the PLD-deposited CoO film was fully capped by an yttria-stabilized zirconia (YSZ) single-crystalline plate to keep the surface clean. Step 3: $NaHCO_3$ powder was put on the YSZ plate. Step 4: The sandwich specimen was annealed at 700 °C for 1 h in air. Notably, several researchers have used this R-SPE method for fabricating Na_xCoO_2 epitaxial films[65–67] since the resultant film quality, especially in surface morphology, is better than that of PLD-grown films[68,69].

The out-of-plane (Fig. 3a) and in-plane (Fig. 3b) X-ray diffraction patterns of the resultant Na_xCoO_2 film clearly indicate that epitaxial growth occurred, showing the effectiveness of the R-SPE method. The chemical composition of the obtained film was evaluated to be $x = 0.83$ by X-ray fluorescence (XRF) measurements. The Na content in the present film was slightly higher than the reported values in the as-grown bulk sample $x = 0.7$[70], likely because the amorphous layer at the interface contained some Na ions[51]. Figure 3c shows an atomic force microscopy (AFM) image of the Na_xCoO_2 film. A step-like structure composed of several flake-like domains could be observed. The step increment was approximately 3 nm, which was three times longer than the c-axis length of Na_xCoO_2, suggesting that step bunching occurred during annealing at 700 °C.

As described in the next section, the R-SPE-grown $Na_{0.7}CoO_2$ epitaxial film was very useful for fabricating epitaxial films of $LiCoO_2$[71], $Sr_{0.5}CoO_2$[52], $Ca_{0.33}CoO_2$[55,72], and $Ca_3Co_4O_9$[55]. Furthermore, the $Na_{0.7}CoO_2$ epitaxial film could be converted into a superconducting sodium cobalt oxyhydrate, $Na_{0.3}CoO_2{\cdot}1.3H_2O$ ($T_c \sim 4$ K), by dipping in HNO_3 for oxidation treatment followed by dipping in NaCl aqueous solution for hydration treatment[73]. Furthermore, peeling-off of the $Na_{0.7}CoO_2$ epitaxial film from the α-Al_2O_3 substrate was possible, and the peeled film could be pasted on the other substrate[51].

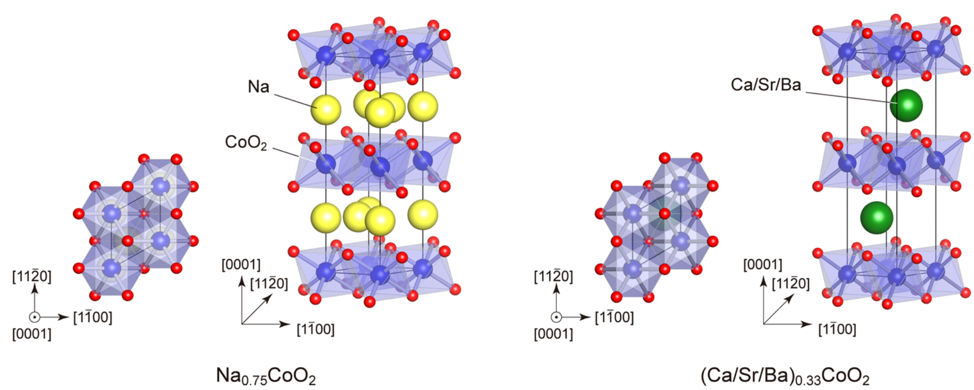

Fig. 1 Schematic illustration of the crystal structure of A_xCoO_2. Left: $A_x = Na_{3/4}$, Right: $A_x = Ca_{1/3}$, $Sr_{1/3}$, and $Ba_{1/3}$.

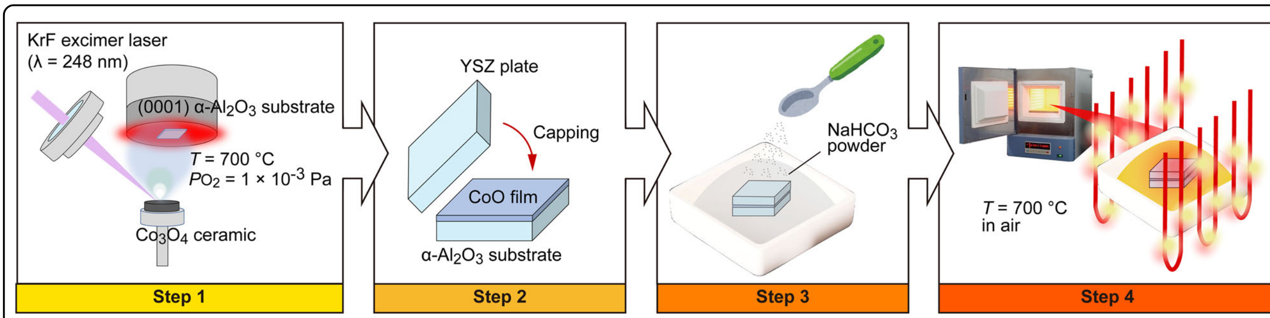

Fig. 2 Film growth procedure. Schematic illustration of reactive solid-phase epitaxy (R-SPE) for the preparation of Na_xCoO_2 epitaxial films.

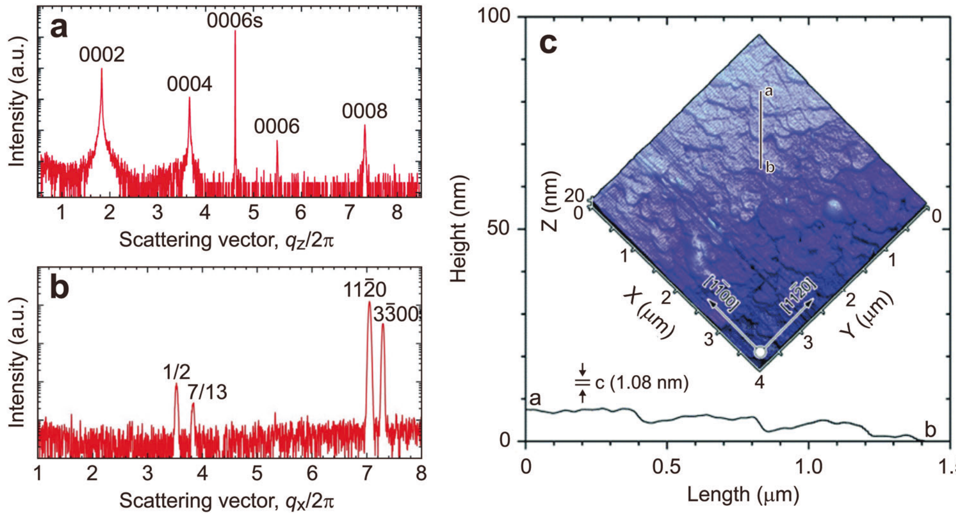

Fig. 3 X-ray diffraction (XRD) patterns and topographic atomic force microscopy (AFM) images of Na_xCoO_2 epitaxial films. a Out-of-plane XRD. **b** In-plane XRD. **c** Topographic AFM image. This figure was reproduced with permission[50,82].

$Ca_{1/3}CoO_2$

Powder syntheses of Ca_xCoO_2 ($x = 0.3$, 0.35 and 0.5) were reported in 1996 by Cushing et al.[74,75] The scholars used specimens of the sodium cobalt oxide Na_xCoO_2 ($0.6 \le x \le 1.0$) as precursors and performed multivalent ion-exchange reactions.

$$Na_xCoO_2 + x/2Ca(NO_3)_2 \rightarrow Ca_{x/2}CoO_2 + x\,NaNO_3$$

Stoichiometric amounts of the A_xCoO_2 precursors were combined with anhydrous $Ca(NO_3)_2$ in evacuated sealed glass tubes and heated at 350 °C for 48 h.

There is an interesting feature in the Ca_xCoO_2 system: there are two superstructures of cation ordering. In 2006, Yang et al. discovered that there are two common well-defined cation ordered states corresponding to the $2a \times \sqrt{3}a$ orthorhombic superstructure at approximately $x = 1/2$ and the $\sqrt{3}a \times \sqrt{3}a$ hexagonal superstructure at approximately $x = 1/3$[76]. In 2006, Sugiura et al. fabricated high-quality $Ca_{0.48}CoO_2$ epitaxial films by ion-exchange reactions. $Na_{3/4}CoO_2$ epitaxial films were heated together with $Ca(NO_3)_2$ powder at 300 °C for 0.5 h in air[55]. In 2008, Huang et al. directly observed two instances of Ca ordering in $Ca_{1/3}CoO_2$ epitaxial films using high-angle annular dark-field (HAADF) scanning transmission electron microscopy (STEM)[77,78].

In 2009, Sugiura et al. found that the structural transformation of $Ca_{1/3}CoO_2$ occurred at approximately 300 °C[72]. The $\sqrt{3}a \times \sqrt{3}a$ hexagonal phase transformed into the $2a \times \sqrt{3}a$ orthorhombic phase when heated in air. The scholars found that the orthorhombic phase showed insulating electron transport, whereas the hexagonal phase showed metallic transport. Interestingly, the temperature dependence of the thermopower of $Ca_{1/3}CoO_2$ epitaxial films was similar, independent of the crystallographic phases.

$Sr_{1/3}CoO_2$

The most serious drawback of $Na_{3/4}CoO_2$ is its low chemical stability against water. $Na_{3/4}CoO_2$ is easily decomposed into insulating $Co(OH)_2$ under high-humidity conditions (temperature, 80 °C; humidity, ~80%) because Na^+ ions can easily dissolve in water. To address this issue, Sugiura and coworkers hypothesized that modification of the chemical composition improves the chemical stability without degrading the thermoelectric performance.

In 2002, Ishikawa et al. reported that the thermoelectric properties of the $Sr_{1/3}CoO_2$ ceramic synthesized by sintering at 400 °C were quite low relative to those of $Na_{3/4}CoO_2$. Although a high-density and single-crystal $Sr_{1/3}CoO_2$ ceramics are preferable for clarifying the intrinsic properties, this process is extremely difficult because the phase transition of $Sr_{1/3}CoO_2$ occurs at a relatively low temperature (~400 °C). To examine the intrinsic thermoelectric properties of $Sr_{1/3}CoO_2$, Sugiura and coworkers fabricated high-quality epitaxial films of $Sr_{1/3}CoO_2$ because epitaxial films generally exhibit intrinsic carrier transport properties, similar to those of bulk single crystals. The $Sr_{1/3}CoO_2$ epitaxial films exhibits better chemical stability than $Na_{3/4}CoO_2$ while retaining good thermoelectric properties.

$Ba_{1/3}CoO_2$

Recently, we found a reliable high-*ZT* thermoelectric oxide, $Ba_{1/3}CoO_2$. The crystal structure and electrical

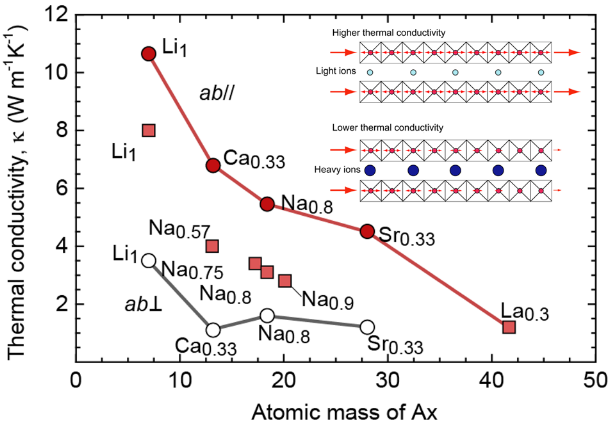

Fig. 4 Reduced thermal conductivity through heavy ion substitution at the A-site of A_xCoO_2. As the mass of the A-site ions increases, the in-plane thermal conductivity ($\kappa_{||}$) and cross-plane thermal conductivity ($\kappa_{\perp}$) show decreasing tendencies. The inset shows a schematic illustration of the phonon propagation of A_xCoO_2. Heavy ions display a stronger thermal conductivity suppression effect than light ions. This figure was reproduced with permission[81].

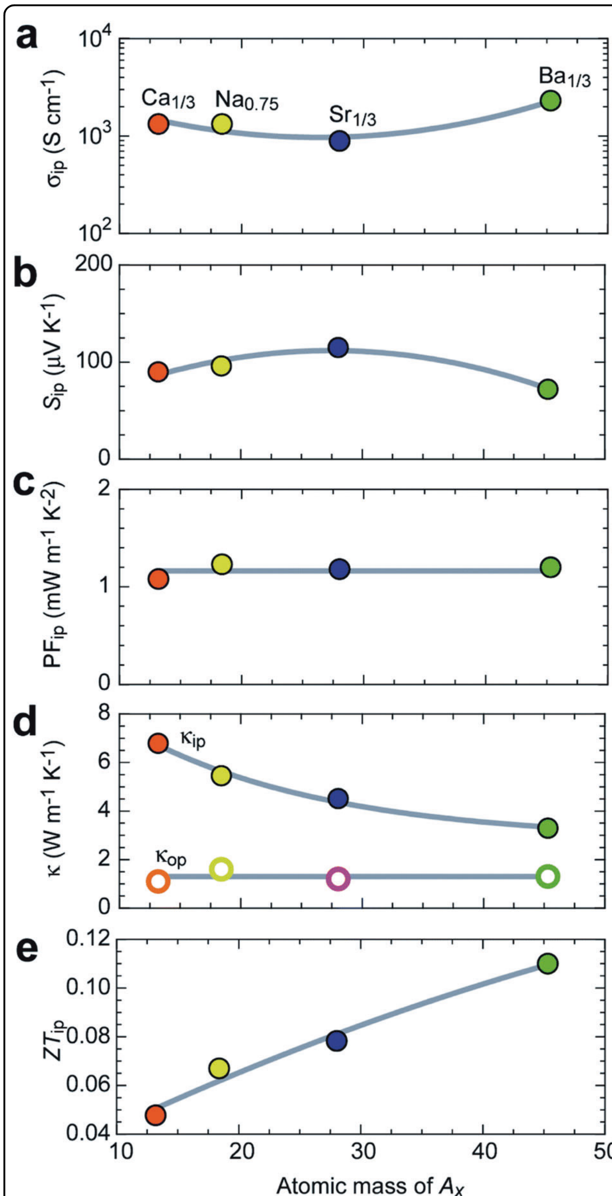

Fig. 5 Thermoelectric properties of A_xCoO_2 epitaxial films at room temperature. a In-plane electrical conductivity (σ_{ip}), **b** in-plane thermopower (S_{ip}), **c** in-plane power factor (PF_{ip}), **d** in-plane and out-of-plane thermal conductivity (κ_{ip}, κ_{op}), and **e** in-plane figure of merit (ZT_{ip}) as a function of the atomic mass A_x in A_xCoO_2. The κ_{ip} shows a clear decreasing tendency, whereas the PF shows a slight increasing tendency. These trends result in an increasing tendency of *ZT*. *ZT* reached 0.11 when $A_x = Ba_{1/3}$. This figure was reproduced with permission[82].

properties of the $Ba_{1/3}CoO_2$ epitaxial films were maintained to 600 °C. The power factor gradually increased to ~1.2 mW m^{-1} K^{-2}, and the thermal conductivity gradually decreased to ~1.9 W m^{-1} K^{-1} with increasing temperature to 600 °C. Consequently, the *ZT* reached ~0.55 at 600 °C in air, which was the highest value among oxides and comparable to those of p-type PbTe and p-type SiGe.

Notably, initial investigations on Ba_xCoO_2-based thermoelectric materials have been conducted by Liu et al.[79,80] The scholars fabricated Ba_xCoO_2 ($x = 0.19$, 0.28, 0.30, 0.33) ceramics by using Ba_xCoO_2 powders synthesized through the ion-exchange technique from $Na_{0.7}CoO_2$. The researchers measured the thermoelectric properties to 800 K and found that *ZT* values ranging from 0.14 to 0.21 were dependent on Ba content. In their research, thermal conductivity did not experience effective suppression from polycrystalline grain boundaries, while electron transport properties deteriorated substantially. Therefore, high-quality epitaxial films are ideal for elucidating the intrinsic properties of Ba_xCoO_2-based thermoelectric materials, which is essential for developing high-performance thermoelectric oxides.

Thermoelectric properties of A_xCoO_2 ($A_x = Na_{3/4}$, $Ca_{1/3}$, $Sr_{1/3}$, and $Ba_{1/3}$) epitaxial films

Systematic investigations on the thermoelectric properties of A_xCoO_2 ($A_x = Na_{3/4}$, $Ca_{1/3}$, $Sr_{1/3}$, and $Ba_{1/3}$) started from our findings that heavy ion substitution at the *A*-site of A_xCoO_2 effectively reduces the in-plane thermal conductivity[81]. By fabricating A_xCoO_2 ($A_x = Li_1$, $Na_{0.75}$, $Ca_{0.33}$, $Sr_{0.33}$, $La_{0.3}$) epitaxial films on (0001) α-Al_2O_3 substrates by conducting R-SPE and an ion exchange process, we clarify the *A*-site ion mass-dependent thermal conductivity of A_xCoO_2[50,51]. As shown in Fig. 4, the in-plane thermal conductivity ($\kappa_{||}$) obviously decreases with the *A*-site ion mass due to the mismatch of the impedance between the cation layer and CoO_2 layers. This impedance hinders coupling of the

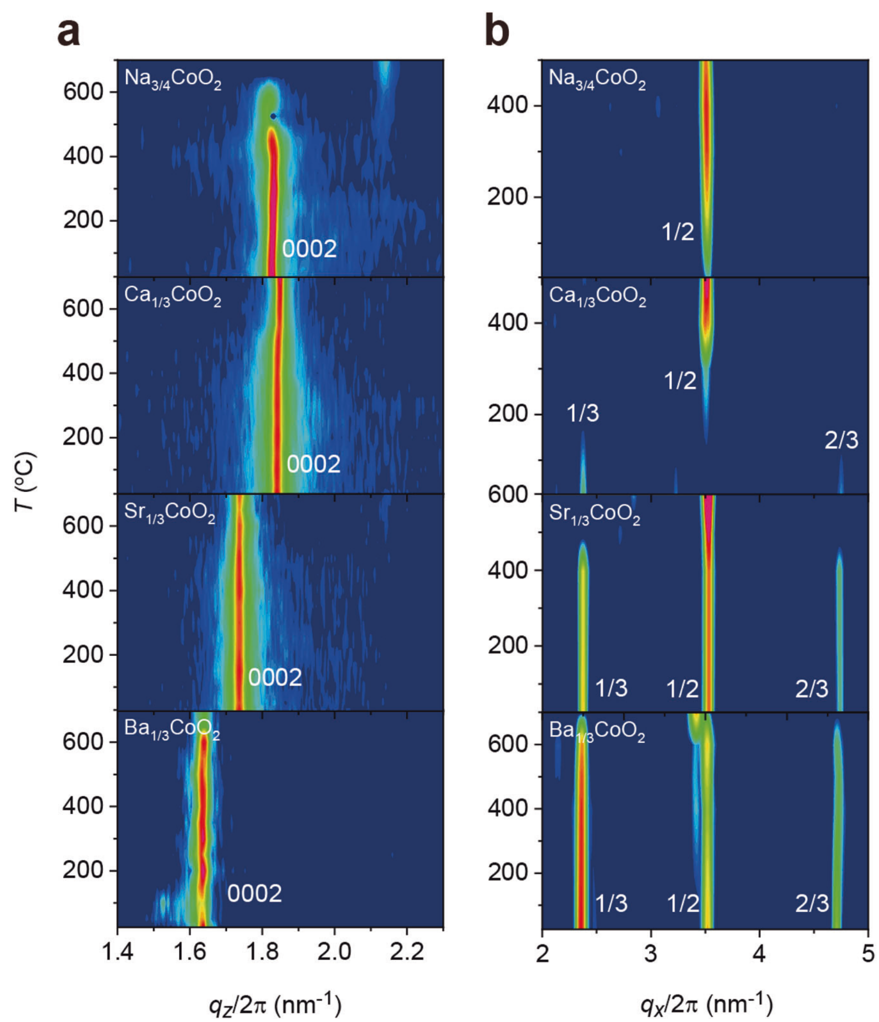

Fig. 6 Changes in the crystal structures of A_xCoO_2 ($A_x = Na_{3/4}$, $Ca_{1/3}$, $Sr_{1/3}$, and $Ba_{1/3}$) films after annealing at high temperatures for 0.5 hours in air. a Out-of-plane XRD patterns measured at room temperature after each annealing step. The 0002 $Na_{3/4}CoO_2$ diffraction peak intensity decreases above 450 °C due to decomposition into Co_3O_4, whereas those for $Ca_{1/3}CoO_2$, $Sr_{1/3}CoO_2$, and $Ba_{1/3}CoO_2$ remain stable to 650 °C. **b** In-plane XRD patterns measured at room temperature after each annealing step. The 1/3 and 2/3 diffraction peaks of the $Ca_{1/3}CoO_2$ film disappear at approximately 200 °C, and the 1/2 diffraction peak appears above 200 °C. The 1/3 and 2/3 diffraction peaks of the $Sr_{1/3}CoO_2$ film disappear at approximately 450 °C, and the 1/2 diffraction peak appears above 450 °C. The 1/3 and 2/3 diffraction peaks of the $Ba_{1/3}CoO_2$ film are stable to 600 °C. This figure was reproduced with permission[54].

vibrational modes, while the cross-plane thermal conductivity ($\kappa_\perp$) mainly depends on the interfacial scattering.

By conducting heavy ion substitution to reduce thermal conductivity, we further fabricate A_xCoO_2 ($A_x = Na_{3/4}$, $Ca_{1/3}$, $Sr_{1/3}$, and $Ba_{1/3}$) epitaxial films on (0001) α-Al_2O_3 and (111) YSZ substrates and compare their room temperature thermoelectric properties[82]. Fig. 5 presents a summary of the room-temperature electrical conductivity (σ_{ip}), thermopower (S_{ip}), power factor (PF_{ip}), thermal conductivity (κ_{ip}) and figure of merit (ZT_{ip}) values along the in-plane direction of A_xCoO_2 epitaxial films. The electrical conductivity and thermopower values of all the films show stable changing patterns, resulting in a consistent power factor (Fig. 5a–c). This consistent value suggests perfect electron–phonon decoupling between the A-site ion layer and CoO_2 layer, where ion substitution has almost no effect on the electrical conductivity of the CoO_2 layers. Moreover, the thermal conductivity along the layered direction decreases with the atomic mass of A_x, thereby enhancing the ZT value (Fig. 5d, e). The highest ZT value of ~0.11 can be obtained in the $Ba_{1/3}CoO_2$ epitaxial film, reaching a peak value among layered cobalt oxides. In this research, the in-plane thermal conductivity has been deduced based on the experimental results of cross-plane thermal conductivities for differently oriented epitaxial films by varying the substrate

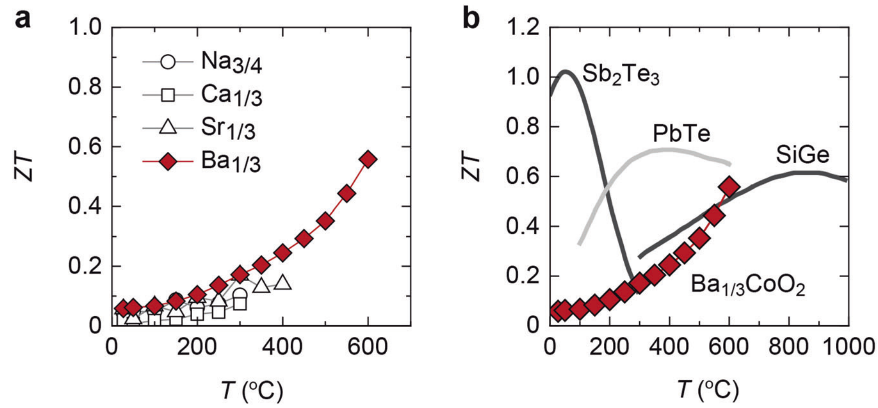

Fig. 7 Temperature dependence of the *ZT* values of $Ba_{1/3}CoO_2$ epitaxial films along the in-plane direction. a Comparison among the four A_xCoO_2 ($A = Na_{3/4}$, $Ca_{1/3}$, $Sr_{1/3}$, and $Ba_{1/3}$) films. In all cases, the *ZT* values increase as the temperature increases. The $Ba_{1/3}CoO_2$ epitaxial film exhibits the highest *ZT* among the four A_xCoO_2 epitaxial films and reaches a *ZT* value of ~0.55 at 600 °C. **b** Comparison against commercially available p-type thermoelectric materials. *ZT* of the $Ba_{1/3}CoO_2$ epitaxial film at 600 °C is comparable to the values of p-type PbTe and p-type SiGe. This figure was reproduced with permission[54].

orientations. In our latest report, we have directly confirmed the in-plane thermal conductivity through AC calorimetric measurements by using a freestanding $Ba_{1/3}CoO_2$ single-crystalline film, yielding a consistent result[83].

As an emerging candidate for high-performance oxide-based thermoelectric materials, $Ba_{1/3}CoO_2$ has promising prospects in applications at elevated temperatures. To elucidate the high-temperature thermoelectric performance, we further conducted high-temperature characterizations of A_xCoO_2 epitaxial films[54]. First, the thermal stabilities of the $Na_{3/4}CoO_2$, $Ca_{1/3}CoO_2$, $Sr_{1/3}CoO_2$, and $Ba_{1/3}CoO_2$ epitaxial films were tested by annealing at an elevated temperature for 0.5 h in air. Figure 6 shows the room temperature XRD patterns after heat treatment. The 0002 $Na_{3/4}CoO_2$ diffraction peak shrinks above 450 °C, whereas the 111 Co_3O_4 peak appears due to the evaporation of Na. In contrast, the 0002 $Ca_{1/3}CoO_2$, 0002 $Sr_{1/3}CoO_2$, and 0002 $Ba_{1/3}CoO_2$ peaks appear below 650 °C (Fig. 6a). However, the in-plane XRD patterns (Fig. 6b) demonstrate that a phase transition from hexagonal to orthorhombic occurs in the $Ca_{1/3}CoO_2$ film when the annealing temperature is above 200 °C[72]. The $Sr_{1/3}CoO_2$ film shows a hexagonal–orthorhombic hybridized phase below 450 °C and a single orthorhombic phase above ~450 °C. Only the $Ba_{1/3}CoO_2$ film can maintain a stable phase composition to 600 °C, which suggests a strong thermal robustness and a high potential for high-temperature $Ba_{1/3}CoO_2$ applications. We have confirmed a similar temperature-dependent behavior from the resistivity variation after heat treatment.

Finally, we calculated the temperature-dependent *ZT* of A_xCoO_2 epitaxial films. The *ZT* values increase with temperature for all films (Fig. 7a). Due to the strongest thermal robustness, the $Ba_{1/3}CoO_2$ epitaxial film displays the highest *ZT* of ~0.55 at 600 °C, which is higher than those of the $Ca_{1/3}CoO_2$ and $Sr_{1/3}CoO_2$ films. This high *ZT* value of $Ba_{1/3}CoO_2$ is reproducible and reliable. This value is comparable to those of p-type PbTe and p-type SiGe, indicating that $Ba_{1/3}CoO_2$ is a suitable candidate for high-temperature thermoelectric applications (Fig. 7b).

Summary and prospects

We have reviewed the thermoelectric properties of representative layered cobalt oxides: A_xCoO_2 (A = Na, Ca, Sr, and Ba) and $Ca_3Co_4O_9$. Although several high-*ZT* thermoelectric oxides ($ZT > 1$) have been reported thus far, their reliability is low due to a lack of careful observation of their stabilities at elevated temperatures. We have explained that $Ba_{1/3}CoO_2$ is stable in air even at 600 °C and exhibits a high *ZT* value of 0.55, which is comparable to p-type PbTe. Bulk crystals (single crystal and sintered) are essential for incorporating $Ba_{1/3}CoO_2$ into thermoelectric conversion elements. To date, we are researching the growth of large single crystals and are proceeding with the production of sintered bodies. Moreover, better thermoelectric performance may be realized by optimizing the compositions and nanostructures of these crystals.

Acknowledgements
The authors thank Drs. Xi Zhang, Hai Jun Cho, Akihiro Tsuruta, Masashi Mikami, and Profs. Yuichi Ikuhara and Bin Feng, and many students at Nagoya University and Hokkaido University for their support. Y.Z. acknowledges the National Natural Science Foundation of China (Grant No. 52202242), the Ministry of Science and Technology of PRC (Grant No. G2022014136L), the National Science Foundation of the Jiangsu Higher Education Institutions of China (Grant No. 22KJB430002), and the Start-Up Fund of Jiangsu University (Grant No. 5501310015). H.O. was supported by Grants-in-Aid for Innovative Areas (19H05791) and Scientific Research A (22H00253) from the Japan Society for the Promotion of Science (JSPS).

Author contributions
H.O. conceived the theme and directed the project. All the authors contributed to writing, reviewing, and editing the manuscript.

Conflict of interest
The authors declare no competing interests.

Publisher's note
Springer Nature remains neutral with regard to jurisdictional claims in published maps and institutional affiliations.

Received: 27 September 2023 Revised: 8 November 2023 Accepted: 14 November 2023.
Published online: 29 December 2023

References

1. Rowe, D. M. *CRC Handbook of TheThe authors declare no competing interestsrmoelectrics*. (CRC Press, 1995).
2. Goldsmid, H. J. *Introduction to Thermoelectricity*. (Springer, 2010).
3. Seebeck, T. J. *Abh. K. Akad. Wiss*. **265** (1823).
4. Tritt, T. M. & Subramanian, M. A. Thermoelectric materials, phenomena, and applications: A bird's eye view. *MRS Bull.* **31**, 188–194 (2006).
5. Snyder, G. J. & Toberer, E. S. Complex thermoelectric materials. *Nat. Mater.* **7**, 105–114 (2008).
6. Venkatasubramanian, R., Siivola, E., Colpitts, T. & O'Quinn, B. Thin-film thermoelectric devices with high room-temperature figures of merit. *Nature* **413**, 597–602 (2001).
7. Zhao, L. D. et al. Ultralow thermal conductivity and high thermoelectric figure of merit in SnSe crystals. *Nature* **508**, 373 (2014).
8. Rhyee, J. S. et al. Peierls distortion as a route to high thermoelectric performance in $In_4Se_{3-\delta}$ crystals. *Nature* **459**, 965–968 (2009).
9. Snyder, G. J., Christensen, M., Nishibori, E., Caillat, T. & Iversen, B. B. Disordered zinc in Zn_4Sb_3 with phonon-glass and electron-crystal thermoelectric properties. *Nat. Mater.* **3**, 458–463 (2004).
10. Zhao, L. D. et al. Ultrahigh power factor and thermoelectric performance in hole-doped single-crystal SnSe. *Science* **351**, 141–144 (2016).
11. Hsu, K. F. et al. Cubic $AgPb_mSbTe_{2+m}$: Bulk thermoelectric materials with high figure of merit. *Science* **303**, 818–821 (2004).
12. Chung, D. Y. et al. $CsBi_4Te_6$: A high-performance thermoelectric material for low-temperature applications. *Science* **287**, 1024–1027 (2000).
13. Kim, S. I. et al. Dense dislocation arrays embedded in grain boundaries for high-performance bulk thermoelectrics. *Science* **348**, 109–114 (2015).
14. Jiang, B. et al. High-entropy-stabilized chalcogenides with high thermoelectric performance. *Science* **371**, 830–834 (2021).
15. Jiang, B. et al. High figure-of-merit and power generation in high-entropy GeTe-based thermoelectrics. *Science* **377**, 208–213 (2022).
16. Zhao, L.-D. et al. BiCuSeO oxyselenides: new promising thermoelectric materials. *Energy Environ. Sci.* **7**, 2900–2924 (2014).
17. Liu, Y. et al. Remarkable Enhancement in Thermoelectric Performance of BiCuSeO by Cu Deficiencies. *J. Am. Chem. Soc.* **133**, 20112–20115 (2011).
18. Yang, J. H. & Stabler, F. R. Automotive Applications of Thermoelectric Materials. *J. Electron. Mater.* **38**, 1245–1251 (2009).
19. Korzhuev, M. A. & Katin, I. V. On the Placement of Thermoelectric Generators in Automobiles. *J. Electron. Mater.* **39**, 1390–1394 (2010).
20. Kim, S. K. et al. Thermoelectric Power Generation System for Future Hybrid Vehicles Using Hot Exhaust Gas. *J. Electron. Mater.* **40**, 778–783 (2011).
21. Vining, C. B. An inconvenient truth about thermoelectrics. *Nat. Mater.* **8**, 83–85 (2009).
22. Koumoto, K. et al. Thermoelectric Ceramics for Energy Harvesting. *J. Am. Ceram. Soc.* **96**, 1–23 (2013).
23. Koumoto, K., Terasaki, I. & Funahashi, R. Complex oxide materials for potential thermoelectric applications. *MRS Bull.* **31**, 206–210 (2006).
24. Koumoto, K., Wang, Y. F., Zhang, R. Z., Kosuga, A. & Funahashi, R. Oxide Thermoelectric Materials: A Nanostructuring Approach. *Annu. Rev. Mater. Res.* **40**, 363–394 (2010).
25. Hogarth, C. A. & Andrews, J. P. Variation with Oxygen Pressure of the Thermoelectric Power of Cadmium Oxide. *Philos. Mag.* **40**, 273–282 (1949).
26. Parravano, G. Thermoelectric Behavior of Nickel Oxide. *J. Chem. Phys.* **23**, 5–10 (1955).
27. Hutson, A. R. Electronic Properties of ZnO. *J. Phys. Chem. Solids* **8**, 467–472 (1959).
28. Arvin, M. J. Electrical Conductivity and Thermoelectric Power of Indium Oxide. *J. Phys. Chem. Solids* **23**, 1681 (1962).
29. Frederikse, H. P. R., Thurber, W. R. & Hosler, W. R. Electronic transport in strontium titanate. *Phys. Rev.* **134**, A442 (1964).
30. Thurber, W. R. & Mante, A. J. H. Thermal Conductivity and Thermoelectric Power of Rutile (TiO_2). *Phys. Rev.* **139**, 1655 (1965).
31. Marley, J. A. & Dockerty, R. C. Electrical Properties of Stannic Oxide Single Crystals. *Phys. Rev.* **140**, A304 (1965).
32. Young, A. P. & Schwartz, C. M. Electrical Conductivity and Thermoelectric Power of Cu_2O. *J. Phys. Chem. Solids* **30**, 249-& (1969).
33. Griffiths, B. A., Elwell, D. & Parker, R. Thermoelectric Power of System $NiFe_2O_4$–Fe_3O_4. *Philos. Mag.* **22**, 163 (1970).
34. Bednorz, J. G. & Muller, K. A. Possible High-*Tc* Superconductivity in the Ba–La–Cu–O System. *Z. Phys. B Con. Mat.* **64**, 189–193 (1986).
35. Cooper, J. R., Alavi, B., Zhou, L. W., Beyermann, W. P. & Gruner, G. Thermoelectric-Power of Some High-T_c Oxides. *Phys. Rev. B* **35**, 8794–8796 (1987).
36. Chen, J. T., Mcewan, C. J., Wenger, L. E. & Logothetis, E. M. Determination of Charge-Carriers in Superconducting La-Ba-Cu-O by Thermoelectric Measurements. *Phys. Rev. B* **35**, 7124–7125 (1987).
37. Lee, S. C. et al. Thermoelectric-Power and Superconducting Properties of $YBa_2Cu_3O_{7-\delta}$ and $RBa_2Cu_3O_{7-\delta}$. *Phys. Rev. B* **37**, 2285–2288 (1988).
38. Mitra, N. et al. Thermoelectric-Power of the Tl-Ca-Ba-Cu-O Superconductor. *Phys. Rev. B* **38**, 7064–7066 (1988).
39. Ohtaki, M., Koga, H., Tokunaga, T., Eguchi, K. & Arai, H. Electrical-Transport Properties and High-Temperature Thermoelectric Performance of $(Ca_{0.9}M_{0.1})MnO_3$ (M = Y, La, Ce, Sm, In, Sn, Sb, Pb, Bi). *J. Solid State Chem.* **120**, 105–111 (1995).
40. Ohtaki, M., Tsubota, T., Eguchi, K. & Arai, H. High-temperature thermoelectric properties of $(Zn_{1-x}Al_x)O$. *J. Appl. Phys* **79**, 1816–1818 (1996).
41. Terasaki, I., Sasago, Y. & Uchinokura, K. Large thermoelectric power in $NaCo_2O_4$ single crystals. *Phys. Rev. B* **56**, 12685–12687 (1997).
42. Masset, A. C. et al. Misfit-layered cobaltite with an anisotropic giant magnetoresistance: $Ca_3Co_4O_9$. *Phys. Rev. B* **62**, 166–175 (2000).
43. Funahashi, R. et al. An oxide single crystal with high thermoelectric performance in air. *Jpn. J. Appl. Phys.* **39**, L1127–L1129 (2000).
44. Okuda, T., Nakanishi, K., Miyasaka, S. & Tokura, Y. Large thermoelectric response of metallic perovskites: $Sr_{1-x}La_xTiO_3$ ($0 \leq x \leq 0.1$). *Phys. Rev. B* **63**, 113104 (2001).
45. Ohta, S., Nomura, T., Ohta, H. & Koumoto, K. High-temperature carrier transport and thermoelectric properties of heavily La- or Nb-doped $SrTiO_3$ single crystals. *J. Appl. Phys.* **97**, 034106 (2005).
46. Ohta, S. et al. Large thermoelectric performance of heavily Nb-doped $SrTiO_3$ epitaxial film at high temperature. *Appl. Phys. Lett.* **87**, 092108 (2005).
47. Fergus, J. W. Oxide materials for high temperature thermoelectric energy conversion. *J. Eur. Ceram. Soc.* **32**, 525–540 (2012).
48. Acharya, M., Jana, S. S., Ranjan, M. & Maiti, T. High performance ($ZT > 1$) n-type oxide thermoelectric composites from earth abundant materials. *Nano Energy* **84**, 105905 (2021).
49. Biswas, S. et al. Selective Enhancement in Phonon Scattering Leads to a High Thermoelectric Figure-of-Merit in Graphene Oxide-Encapsulated ZnO Nanocomposites. *ACS Appl. Mater. Interfaces* **13**, 23771–23786 (2021).
50. Ohta, H. et al. Reactive solid-phase epitaxial growth of Na_xCoO_2 (x ~0.83) via lateral diffusion of Na into a cobalt oxide epitaxial layer. *Cryst. Growth Des.* **5**, 25–28 (2005).
51. Ohta, H. et al. Surface modification of glass substrates for oxide heteroepitaxy: Pasteable three-dimensionally oriented layered oxide thin films. *Adv. Mater.* **18**, 1649 (2006).
52. Sugiura, K. et al. Fabrication and thermoelectric properties of layered cobaltite, γ-$Sr_{0.32}Na_{0.21}CoO_2$ epitaxial films. *Appl. Phys. Lett.* **88**, 082109 (2006).
53. Sugiura, K. et al. Thermoelectric properties of the layered cobaltite $Ca_3Co_4O_9$ epitaxial films fabricated by topotactic ion-exchange method. *Mater. Trans.* **48**, 2104–2107 (2007).
54. Zhang, X. et al. $Ba_{1/3}CoO_2$: A Thermoelectric Oxide Showing a Reliable ZT of ~0.55 at 600 °C in Air. *ACS Appl. Mater. Interfaces* **14**, 33355–33360 (2022).
55. Sugiura, K. et al. High electrical conductivity of layered cobalt oxide $Ca_3Co_4O_9$ epitaxial films grown by topotactic ion-exchange method. *Appl. Phys. Lett.* **89**, 032111 (2006).

56. Kurita, D., Ohta, S., Sugiura, K., Ohta, H. & Koumoto, K. Carrier generation and transport properties of heavily Nb-doped anatase TiO_2 epitaxial films at high temperatures. *J. Appl. Phys.* **100**, 096105 (2006).
57. Lee, K. H., Ishizaki, A., Kim, S. W., Ohta, H. & Koumoto, K. Preparation andthermoelectric properties of heavily Nb-doped $SrO(SrTiO_3)_1$ epitaxial films. *J. Appl. Phys.* **102**, 033702 (2007).
58. Singh, D. J. Electronic structure of $NaCo_2O_4$. *Phys. Rev. B* **61**, 13397–13402 (2000).
59. Koshibae, W. & Maekawa, S. Electronic state of a CoO layer with hexagonal structure: A Kagome lattice structure in a triangular lattice. *Phys. Rev. Lett.* **91**, 257003 (2003).
60. Koshibae, W. & Maekawa, S. Effects of spin and orbital degeneracy on the thermopower of strongly correlated systems. *Phys. Rev. Lett.* **87**, 236603 (2001).
61. Wang, Y. Y., Rogado, N. S., Cava, R. J. & Ong, N. P. Spin entropy as the likely source of enhanced thermopower in $Na_xCo_2O_4$. *Nature* **423**, 425–428 (2003).
62. Lee, M. et al. Large enhancement of the thermopower in Na_xCoO_2 at high Na doping. *Nat. Mater.* **5**, 537–540 (2006).
63. Fujita, K., Mochida, T. & Nakamura, K. High-temperature thermoelectric properties of $Na_xCoO_{2-\delta}$ single crystals. *Jpn. J. Appl. Phys.* **40**, 4644–4647 (2001).
64. Takada, K. et al. Superconductivity in two-dimensional CoO_2 layers. *Nature* **422**, 53–55 (2003).
65. Venimadhav, A. et al. Structural and transport properties of epitaxial Na_xCoO_2 thin films. *Appl. Phys. Lett.* **87**, 172104 (2005).
66. Chang, W. J. et al. Fabrication and low temperature thermoelectric properties of Na_xCoO_2 (x = 0.68 and 0.75) epitaxial films by the reactive solid-phase epitaxy. *Appl. Phys. Lett.* **90**, 061917 (2007).
67. Sugiura, K. et al. Anisotropic carrier transport properties in layered cobaltate epitaxial films grown by reactive solid-phase epitaxy. *Appl. Phys. Lett.* **94**, 152105 (2009).
68. Krockenberger, Y. et al. Epitaxial growth of Na_xCoO_2 thin films by pulsed-laser deposition. *Appl. Phys. Lett.* **86**, 191913 (2005).
69. Brinks, P. et al. Enhanced Thermoelectric Power Factor of Na_xCoO_2 Thin Films by Structural Engineering. *Adv. Energy Mater.* **4**, 201301927 (2014).
70. Lee, M. et al. Enhancement of the thermopower in Na_xCoO_2 in the large-x regime ($x \geq 0.75$). *Phys. B* **403**, 1564–1568 (2008).
71. Mizutani, A., Sugiura, K., Ohta, H. & Koumoto, K. Epitaxial film growth of Li_xCoO_2 ($0.6 \leq x \leq 0.9$) via topotactic ion exchange of $Na_{0.8}CoO_2$. *Cryst. Growth Des.* **8**, 755 (2008).
72. Sugiura, K. et al. Structural Transformation of Ca-Arrangements and Carrier Transport Properties in $Ca_{0.33}CoO_2$ Epitaxial Films. *Appl. Phys. Express* **2**, 035503 (2009).
73. Sugiura, K. et al. Epitaxial film growth and superconducting behavior of sodium-cobalt oxyhydrate, Na_xCoO_2-$y$$H_2O$ (x ~0.3, y ~1.3). *Inorg. Chem.* **45**, 1894–1896 (2006).
74. Cushing, B. L., Falster, A. U., Simmons, W. B. & Wiley, J. B. A multivalent ion exchange route to lamellar calcium cobalt oxides, Ca_xCoO_2 ($x \leq 0.5$). *Chem Commun* **23**, 2635–2636 (1996).
75. Cushing, B. L. & Wiley, J. B. Topotactic routes to layered calcium cobalt oxides. *J. Solid State Chem.* **141**, 385–391 (1998).
76. Yang, H. X. et al. Structural properties and cation ordering in layered hexagonal Ca_xCoO_2. *Phys. Rev. B* **73** (2006).
77. Huang, R. et al. Direct observations of Ca ordering in $Ca_{0.33}CoO_2$ thin films with different superstructures. *Appl. Phys. Lett.* **93**, 014109 (2008).
78. Huang, R. et al. Microstructure evolution of $Ca_{0.33}CoO_2$ thin films investigated by high-angle annular dark-field scanning transmission electron microscopy. *J. Mater. Res.* **24**, 279–287 (2009).
79. Liu, J., Huang, X., Yang, D., Xu, G. & Chen, L. Synthesis and physical properties of layered Ba_xCoO_2. *Dalton Trans.* **43**, 15414 (2014).
80. Liu, J., Huang, X., Yang, D., Wan, S. & Xu, G. High-temperature thermoelectric properties of layered Ba_xCoO_2. *Scr. Mater.* **100**, 63–65 (2015).
81. Cho, H. J., Takashima, Y., Nezu, Y., Onozato, T. & Ohta, H. Anisotropic Heat Conduction in Ion-Substituted Layered Cobalt Oxides. *Adv. Mater. Interfaces* **7**, 1901816 (2020).
82. Takashima, Y. et al. Layered Cobalt Oxide Epitaxial Films Exhibiting Thermoelectric $ZT = 0.11$ at Room Temperature. *J. Mater. Chem. A* **9**, 274–280 (2021).
83. Kang, K. et al. Fabrication and Thermoelectric Properties of Freestanding $Ba_{1/3}CoO_2$ Single-Crystalline Films. *ACS Appl. Electron. Mater.* **5**, 5749–5754 (2023).